Available online at www.sciencedirect.com
SCIENCE DIRECT®
Journal of Electron Spectroscopy and Related Phenomena 144–147 (2005) 259–269
JOURNAL OF ELECTRON SPECTROSCOPY and Related Phenomena
www.elsevier.com/locate/elspec

# Soft X-ray spectromicroscopy of biological and synthetic polymer systems

Adam P. Hitchcock [a,*], Cynthia Morin [a], Xuerong Zhang [a], Tohru Araki [a,1], Jay Dynes [a], Harald Stöver [a], John Brash [a], John R. Lawrence [b], Gary G. Leppard [c]

[a] *Brockhouse Institute of Materials Research, McMaster University, Hamilton, Ont., Canada L8S 4M1*
[b] *National Water Research Institute, 11 Innovation Blvd, Saskatoon, Sask., Canada S7N 3H5*
[c] *National Water Research Institute, 867 Lakeshore Road, P.O. Box 5050, Burlington, Ont., Canada L7R 4A6*

Available online 3 March 2005

**Abstract**

Scanning transmission X-ray microscopy (STXM) and X-ray photoemission electron microscopy (X-PEEM) are synchrotron based, soft X-ray spectromicroscopy techniques, which provide chemical speciation at better than 50 nm spatial resolution based on near edge X-ray absorption spectral (NEXAFS) contrast. The instrumentation and acquisition protocols for these microscopies are described. Methods for converting image sequences to quantitative maps of chemical components are outlined and illustrated with applications to characterization of wet biofilms, optimization of the microstructure of synthetic polymers, and studies of protein interactions with patterned polymer surfaces.
© 2005 Elsevier B.V. All rights reserved.

*Keywords:* Soft X-ray microscopy; NEXAFS; STXM; PEEM; Biofilms; Microspheres; Tectocapsules; Biomaterials

## 1. Introduction

Soft X-ray spectromicroscopy is rapidly developing with the continual increases in the availability of high brightness third generation light sources and improvements in instrumentation. One of the major advantages relative to other analytical microscopies is the ability to use the *intrinsic* properties of the sample, through the near-edge X-ray absorption fine structure (NEXAFS) signal [1], as the analytical contrast mechanism. This requires a source of bright, continuously tunable soft X-rays (50–2000 eV), and thus synchrotron radiation is uniquely suited. Magnetic structures can be imaged using X-ray magnetic circular dichroism and orientation can be imaged via linear polarization. Soft X-ray spectromicroscopy is being used for chemically sensitive imaging and quantitation in a wide range of specimens, such as nanostructured synthetic polymers, fully hydrated environmental and biological specimens, and magnetic materials. Many of these systems were previously difficult or impossible to study by other means, for reasons, such as inadequate spatial resolution in the case of IR, NMR and optical techniques; inability to couple to wet specimens in the case of electron beam based techniques; radiation damage in the case of electron microscopy; lack of chemical sensitivity in scanning probe techniques.

There are many different soft X-ray microscopy techniques. One can divide these into full field techniques, such as transmission X-ray microscopy (TXM) [2,3] and X-ray photoemission electron microscopy (X-PEEM) [4–6], and scanning techniques, based on focusing X-rays to a small spot using Kirkpatrick–Baez or other mirror technologies or Fresnel zone plates as used in scanning transmission X-ray microscopy (STXM) and scanning photoemission microscopy (SPEM) [7,8]. There are several recent reviews of soft X-ray microscopy [2,7,8], and the published proceedings of the triannual conference on X-ray microscopy [9] are an excellent source of information on the latest capabilities and applications. Here, we describe our work with two methods of soft

* Corresponding author. Tel.: +1 905 525 9140x24749; fax: +1 905 521 2773.
*E-mail address:* aph@mcmaster.ca (A.P. Hitchcock).
[1] Present address: Department of Physics, North Carolina State University, Raleigh, NC 27695, USA

0368-2048/$ – see front matter © 2005 Elsevier B.V. All rights reserved.
doi:10.1016/j.elspec.2005.01.279

X-ray spectromicroscopy – STXM and X-PEEM – with focus on quantitative chemical speciation in natural (primarily biological) and synthetic polymer systems.

While many chemical analysis problems can be resolved through qualitative comparisons of chemically sensitive images, soft X-ray microscopy provides its greatest impact when spectra and images are analyzed quantitatively. NEXAFS spectra of pure samples of the individual components (or close analogs) on an absolute response scale provide suitable quantitative reference standards. The most extensive information is obtained from image sequences [10], which can be analyzed to derive quantitative component maps (spatial distributions of the concentration of each component) and associated color-coded composite representations to explore spatial correlations of components, as is illustrated in examples below. In many cases, quantitative spatial correlations are the key to resolving a scientific problem.

## 2. Experimental

Fig. 1 is a sketch of the interferometrically controlled STXM [11] located at bend magnet beamline 5.3.2 [12] at the Advanced Light Source (ALS). A second version of the interferometric-STXM is now working on undulator beamline 11.0.2 at the ALS [13]. A similar interferometeric-STXM is under construction at the elliptically polarized undulator beamline 10ID1 at the Canadian Light Source. The 5.3.2 beamline is very simple with only two optical surfaces, a toroidal mirror to focus the light emitted by a few percent of the horizontal swath emitted by a bend magnet, and a spherical grating which disperses the light horizontally. The optical parameters were carefully selected to match the phase space of the source (physical size × angular divergence) to the sub-200 micron zone plates, thus preserving brightness. The beamline delivers monochromated light to the zone plate through a rectangular exit aperture, which acts as a pinhole to define transverse coherence. A silicon nitride window separates the STXM chamber (which operates in air, He, or coarse vacuum) from the ultrahigh vacuum of the beamline. The STXM (Fig. 1c) consists of the zone plate (ZP) (currently 150 μm diameter, 35 nm outer zone, 80 μm central stop, with a diffraction limited resolution of 42 nm), a 55 μm diameter order sorting aperture (OSA), which works with the central stop to block zero order light, the sample scan stages, and a transmitted detector. Transmitted X-rays are converted to visible light pulses and detected with a photomultiplier operated in counting mode. Typical incident flux levels at full spectral (100 meV) and spatial (42 nm) resolution are 1–2 MHz in the C 1s region rising to 10–20 MHz in the N 1s region. With modest degradation of either spectral or spatial resolution (user selectable), the flux in the spot on the sample can be ∼10 times higher. Images are acquired pixel-by-pixel using dwells between 0.5 and 2 ms/pixel. The beamline provides light from 180 to 1200 eV, although it has optimum performance between 250 and 550 eV due to a fixed exit slit position. A sophisticated interferometer system [11] is used to control the (*x*, *y*) position of the sample relative to the zone plate (and thus focused X-ray spot) with a precision of 10 nm, thus providing accurate positioning in point spectra mode, and stable fields of view in imaging mode, even though the zone plate-sample separation might be changed by a millimeter or more in a NEXAFS scan. Samples for STXM must be partially X-ray transparent, with optimum optical densities between 0.3 and 2. For unit density materials, this corresponds to ∼100 nm thickness for C 1s and ∼500 nm thickness for O 1s studies. Techniques for preparing the thin section samples are similar to those used for transmission electron microscopy. Fully solvated samples are examined by sandwiching the wet sample between two X-ray translucent silicon nitride windows. Thicknesses of water (or other solvents) up to 3 or 4 μm can be tolerated.

Data are collected as single energy images, point spectra, linescan spectra, and image sequences. Image sequences, pi-

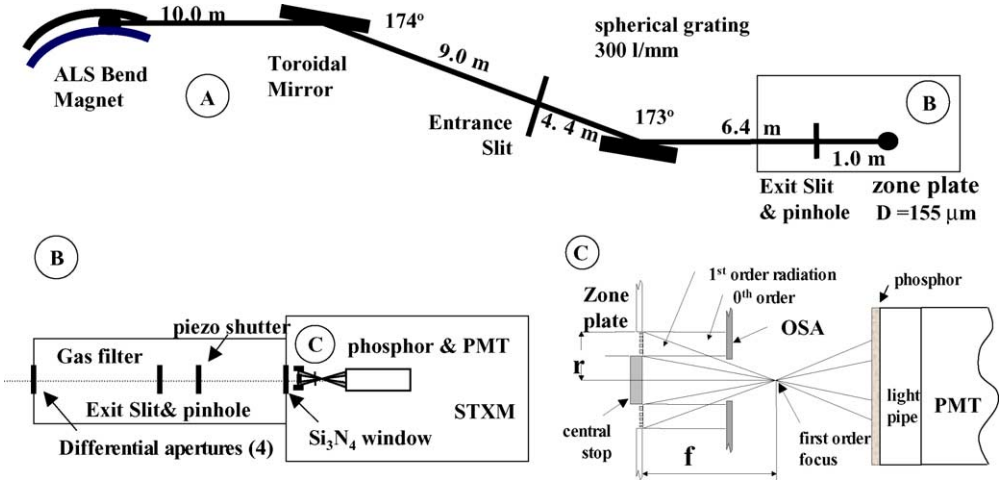


Fig. 1. Schematic of beamline 5.3.2 and the interferometrically controlled STXM (referred to as 'STXM5.3.2'). (a) Beamline; (b) in-hutch components (gas filter, exit slit, fast shutter and STXM); (c) details of the STXM optics.

oneered in STXM by Jacobsen et al. [10], provide the most detailed information about a sample, and are the basis for quantitative chemical mapping. For quantitative analysis, the transmitted signal is converted to absorbance (A), also called optical density (OD),

$$\mathrm{OD}(E) = \ln\left(\frac{I_0}{I}\right) = \mu(E)\rho t = \sigma(E)t \quad (1)$$

where for a given X-ray energy, $E$, $I_0$ is the incident X-ray flux, $I$ the transmitted flux through the sample, $\mu(E)$ the mass absorption coefficient at X-ray energy $E$, $\rho$ the density, $t$ the sample thickness, and $\sigma(E)$ is the linear absorption coefficient. The mass or linear absorption coefficients are derived from the NEXAFS spectra of the pure material (typically recorded in the same apparatus) using the well-characterized elemental response outside the near edge region [14] to set the scale.

## 3. Quantitative chemical mapping by analysis of image sequences

The image sequence analysis procedure can be applied to any type of spectromicroscopy (e.g. infrared, visible light, as well as a wide variety of X-ray microscopies). It computes a least squares fit of the intensity at each pixel – $S(j, k)$ – to a linear combination of reference spectra for each component ($S_i$, each on a quantitative linear absorption scale).

$$S(j, k) = a_0(j, k) + \sum\nolimits_{\mathrm{i}} a_i(j, k) \times S_i \quad (2)$$

The fit coefficient, $a_i$ is the equivalent thickness (in nm, if the reference spectra are in linear absorption format with units of $\mathrm{nm}^{-1}$) of the $i$th component at the ($j$, $k$) pixel and the concentration at that point is given by $a_i/\Sigma_i a_i$ ($j$, $k$). The inversion of the image sequence to component maps – the set of $a_i$ ($j$, $k$) values – is conveniently carried out using matrix techniques available as part of a user-friendly graphical interface, aXis2000 [15]. In the stack fit approach an energy independent term, ($a_0$) is included, which accounts for energy independent offsets (backgrounds) in the reference or the image sequence spectra. In the singular value decomposition (SVD) approach [16–18], there is no $a_0$ term. It is usually a good idea to compare the results from each method. In a robust analysis, the component maps derived from the two approaches are very similar, and the map of the constant term is featureless, with a histogram centered about 0. In addition to the component maps, the implementation of this methodology provides several other useful tools to assist the analyst. A map of the energy-averaged residuals (the least squares measure of the mis-match between the actual spectrum and the fit at each pixel) is generated. It is also possible to save an image sequence of the residuals, which in favorable cases, allows one to identify missing chemical components by examination of the spectrum of the regions of poor fit. aXis2000 [15] provides tools to identify pixels with user specified properties (i.e. those in a component map that exceed a certain value which correspond to regions of high concentration of that component), to extract the average spectra of those pixels, and then to fit the extracted spectrum in order to examine in greater detail the spectral match of the unknown and the set of weighted reference spectra.

Fig. 2 is an example of quantitative chemical mapping using image sequence analysis as described above. The sample is a core shell microsphere [19,20] consisting of a 3 μm diameter cross-linked divinylbenzene (DVB) core, with a ∼600 μm shell of pure ethylene glycol dimethyl acrylate (EGDMA) subsequently added. These microspheres are embedded in an aliphatic epoxy and microtomed to about 100 nm thickness. While a number of embedding materials can and have been used, this formulation was specifically chosen for good embedding properties for a range of polymer systems, a NEXAFS spectrum that has minimal structure and thus limited interference with NEXAFS-based analysis, and a high tolerance to radiation [21]. Eighty images (each 6 μm × 6 μm, 175 pixels × 175 pixels; 1 ms/pixel dwell) were acquired between 280 and 315 eV. Spectra extracted from the three chemically distinct regions of the image sequence are displayed in Fig. 2a. These have been converted to linear absorption scale (using longer range spectra acquired separately to set the intensity scale) and used as the models for the quantitative analysis. Images at four characteristic energies are presented in Fig. 2b–e to show the dramatic changes in contrast, which relate to the difference in the chemical structure of the epoxy, DVB and EGDMA components. The component maps derived from SVD of all 80 images are combined to form a color coded composite map (Fig. 2f), constructed by using the byte-scaled epoxy map for the red component, the byte-scaled DVB map for the green component, and the byte-scaled EGDMA map for the blue component. Color composite maps can be constructed either byte scaled or with preservation of the relative thickness scale, by using a single intensity scale, set by the overall minima and maxima of the three component maps. The former is called a ‘scaled composite map’ and the latter an ‘un-scaled composite map’. Each approach has its uses; the scaled map best displays the location of each component, even if there is a large difference in amounts, while the un-scaled map gives a true quantitative picture. In this system, where the components each have similar thickness and are completely spatially separated, the scaled and un-scaled composite maps look similar.

Additional methods can be used to assist analysis of soft X-ray microscopy image sequences. Principle component analysis [22,23] allows one to estimate the number of statistically accessible spectral components in a system. Jacobsen and co-workers [24] have recently developed elegant methods to combine principle component (factor) analysis with an optimized cluster analysis to provide means to extract suitably orthogonalized spectra of chemical components from image sequences without prior knowledge of the components present, or their NEXAFS spectrum.

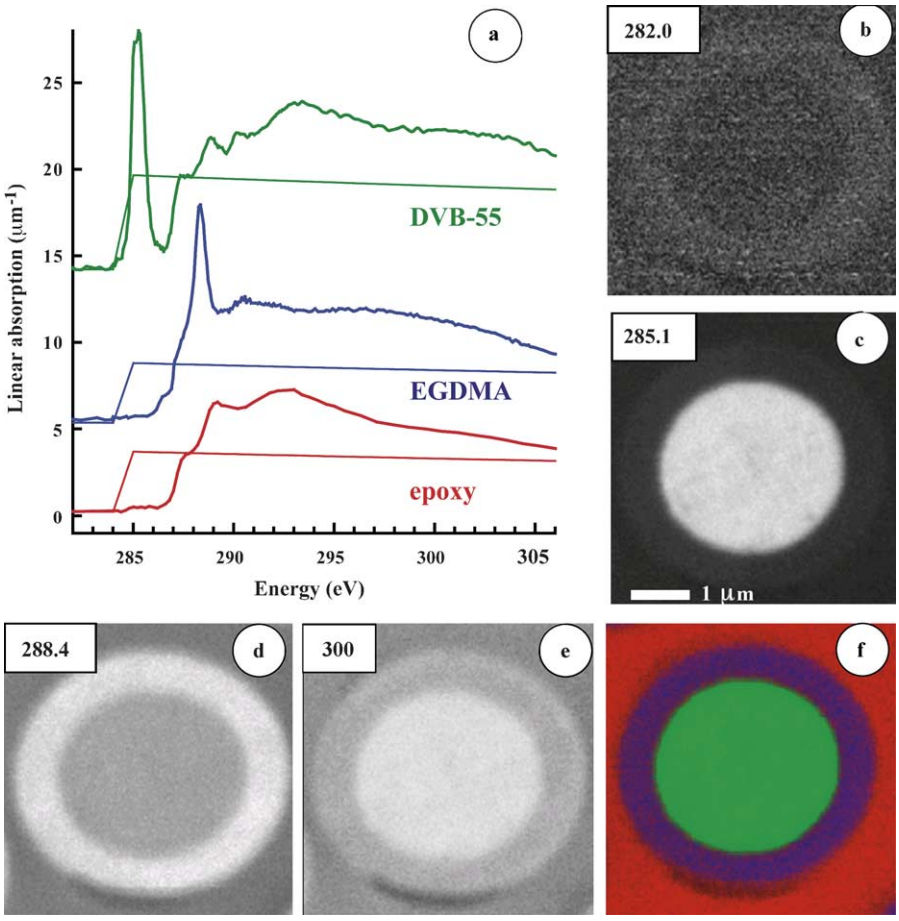


Fig. 2. (a) C 1s spectra of divinylbenzene (DVB), ethylene glycol dimethylacrylate (EGDMA), and an aliphatic epoxy, converted to linear absorption scales by matching to the elemental response (thin lines) outside of the near edge structured region. (b–e) Optical density (OD) images at selected energies of a core-shell polymer consisting of a pure DVB core, a 100% EGDMA shell, embedded in the aliphatic epoxy. (f) Re-scaled color coded composite derived from the C 1s image sequence (epoxy: red, DVB: green, EGDMA: blue) (recorded with STXM5.3.2).

## 4. Natural polymer systems

Living species rarely exist in isolation. At the 0.1–100 micron scale of microbes – bacteria, algae, fungi, cyanobacteria, etc. – it is common for individuals from single or several different species to form colonies linked by extracellular polymeric substances (EPS). Although EPS are mainly microbial polysaccharides, other biochemical macromolecules – proteins, nucleic acids and polymeric lipophilic compounds – have been identified and are suspected to play important roles. EPS represent a major structural component of biofilms and are known to be responsible for sorption processes used to provide nutrients to the living entities and to help control exposure to toxic metal and organic substances [25,26]. Particularly in complex environmental systems, the EPS are difficult to characterize by isolating single polymer species. Increasingly, in situ methods are being used to examine the EPS of natural biofilms. STXM wet cell techniques are particularly powerful for studies of fully hydrated biological and environmental materials. STXM provides better spatial resolution than optical techniques and chemical information at a microscale relevant to bacteria. Using the intrinsic X-ray absorption properties of the sample avoids addition of reflective, absorptive, or fluorescent probes and markers, which may introduce artifacts or complicate interpretation. We use STXM to characterize the biochemical and abiotic components of biofilms. We have mapped protein, nucleic acids, lipids and polysaccharides in riverine biofilm systems [27], and have studied the distribution of metal species in biofilms [13], which have been exposed intentionally to part-per-million concentrations of metal ions, such as nickel chloride.

Fig. 3 presents STXM images of a wet, riverine biofilm recorded at several spatial scales using 288.2 eV, a photon energy which highlights the biological components through the strong amide protein absorption band. The sample consists of a silicon nitride wet cell with a 1 mm × 1 mm viewing area. The whole sample is imaged in Fig. 3a while expanded images are given in Fig. 3b and c. This illustrates the complexity and diversity of these samples and also indi-

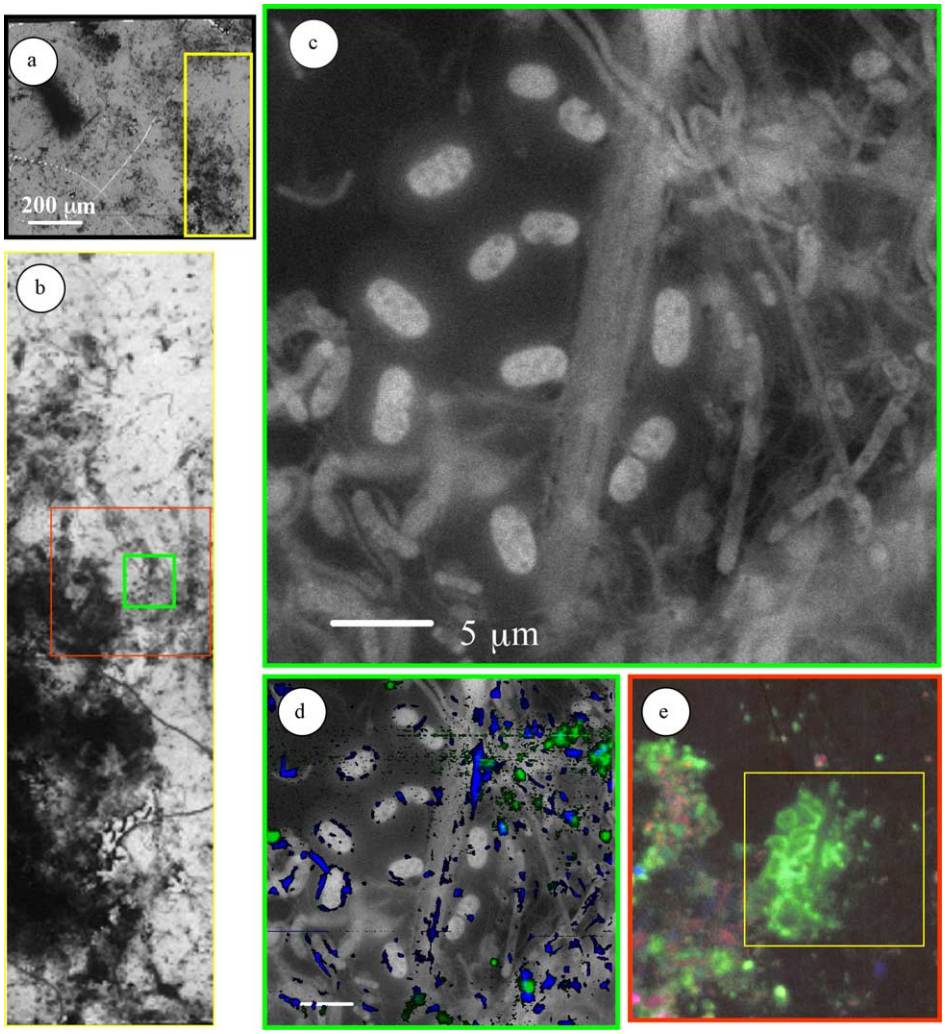


Fig. 3. (a) Transmission image of the full wet cell of a river water biofilm sample recorded at 288.2 eV recorded with STXM5.3.2. (b) Transmission image of right-most 150 μm × 1000 μm for this sample. (c) OD image of area D, a microbial colony adjacent to a diatom skeleton (288.2 eV). (d) Overlay of Ca ($I_{352}$–$I_{350}$) (blue) and Fe ($I_{709}$–$I_{706}$) (green) component maps on to the 288.2 eV image. (e) Laser confocal scanning micrograph of the same region. The sample was stained with *Ulex europeaus*-FITC conjugated lectin with sensitivity to fucose, sealed, and imaged by CLSM prior to X-ray microscopy.

cates some of the challenges involved. A typical field of view for detailed studies is 20 μm × 20 μm, so there are a huge number of possible local environments to explore in detail. This particular sample has many well-developed biofilm environments with a thickness and density suitable for STXM. Area D (Fig. 3c), a set of bacteria lying beside the silicaceous skeleton of a diatom, has been studied in the regions of C 1s, Ca 2p, N 1s, O 1s, Mn 2p, Fe 2p and Ni 2p edges. Fig. 3d is a map of Ca (blue, difference of images recorded on/off the Ca $2p_{1/2}$ resonance at 352.6 eV) and Fe (green, difference of images recorded on/off the Fe $2p_{1/2}$ resonance at 709 eV) superimposed on the OD image at 288.2 eV. The STXM results are also compared to a confocal laser scanning microscopy (CLSM) image of the same region (Fig. 3e). In CLSM, laser excited fluorescence from lectin dyes is used to locate specific polysaccharides in the extra-cellular matrix. STXM and CLSM provide complementary information. CLSM has very sensitive, tunable sensitivity to specific biomolecules and the ability to perform three dimensional imaging of wet biofilms. STXM uses intrinsic spectral contrast, which avoids possible artifacts intrinsic to the biochemical labeling, can sense essentially all species present, and has higher spatial resolution than CLSM.

Fig. 4 presents quantitative maps of three of the major components – proteins, polysaccharides and lipids – derived from a six component stack fit to a 52-image C 1s sequence (282–315 eV) recorded with STXM5.3.2 in area D for which the 288.2 eV OD image is shown in Fig. 3c. The six reference spectra are plotted in Fig 4a. A major challenge is to identify the correct set of reference spectra to properly identify and map the components. Not only does one have to be careful that the spectra are correct for the species present in the region examined, but also the number of model spectra needs to be large enough to fit the significant variance in the data, but

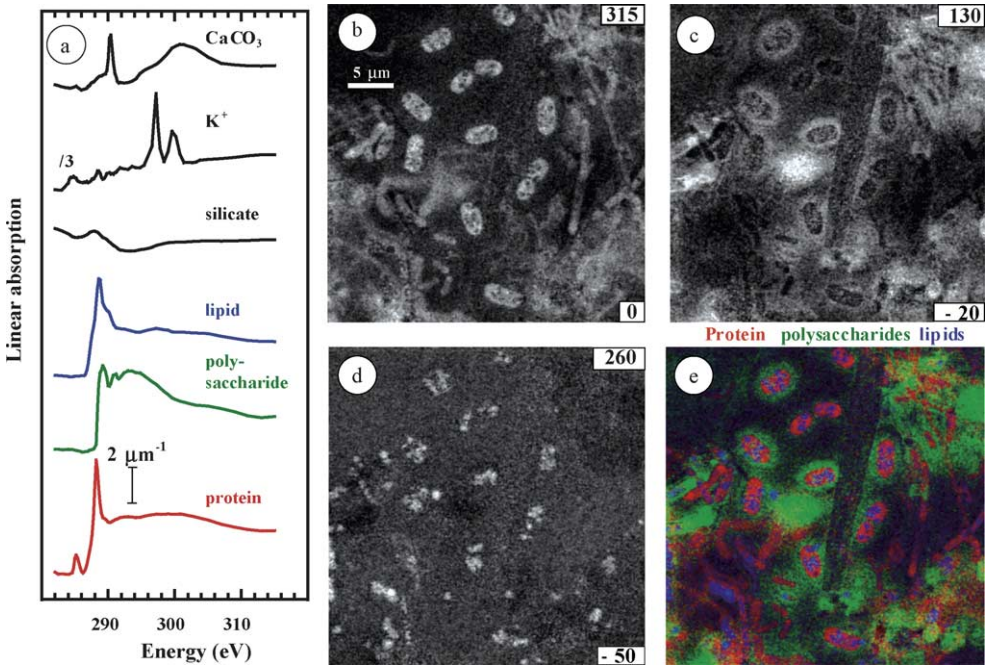


Fig. 4. (a) C 1s spectra of six components used to map chemical species in region D of the riverine biofilm. These spectra are derived from selected regions of the image sequence using spectra of pure materials as a guide. Quantitative component maps (right hand numbers indicate grayscale thickness limits in nanometer) for (b) the protein, (c) polysaccharide and (d) lipid components, along with (e) a scaled color coded composite of these three components, derived from a fit to the C 1s image sequence using the six components indicated in panel (a) (recorded with STXM5.3.2).

without using so many components that the analysis becomes over-determined. At present, we use a trial-and-error strategy to find the set of reference spectra which just accounts for most of the variance of the data, as indicated by minimizing the magnitude and structure of the residual map. This procedure could be greatly assisted by the factor analysis approach [24]. The component maps (Fig. 4) indicate that the chemical structure of the bacterial cells, including the EPS matrix and other biofilm materials are quite complex. Although space does not permit details, we have used STXM11.0.2 to detect regions with various oxidation states of Fe, Ni and Mn in association with bacterial species in this same biofilm sample [13]. The mapping of Ca and Fe (Fig. 3d) illustrates the potential to study biomineralization phenomena. Other recent biomineralization studies by soft X-ray microscopy are STXM studies of Mn nodules and other environmental systems by Tonner and co-workers [28,29], full field TXM to examine biofilm formation [30], and X-PEEM to investigate bio-mineralization in archaeo-bacteria colonies [31].

## 5. Synthetic polymer systems

Increasingly, sophisticated chemical organization of polymers on the micro- and nano-scale is used to achieve desired properties. For example, core-shell structures like that in Fig. 2 are being evaluated for controlled release of pheromones for biological based agricultural pest control [32], capsules constructed from polyurethanes are used as adhesives, modified alginate capsules are used for drug delivery applications [33], and novel structures self-assembled from polymer blends and grafts are being developed as potential optical devices [34,35]. The properties of these systems – compatibility, release rate, resistance to a specific environment – are optimized for a given application by tuning the porosity and chemistry of the barrier. We are using STXM to assist optimization of a number of these systems [33,35,36]. An interesting recent example is ‘tectocapsules’ [37], a novel system for controlled release in which two different encapsulation technologies – microspheres and capsules – are combined in a way that allows the barrier functionality to be determined by the capsule chemistry, while the release functionality is controlled by the properties of porous microspheres embedded in the impermeable capsule wall. Fig. 5 sketches the ‘tectocapsule’ concept. Initial attempts to combine these materials resulted in samples where the microsphere release elements were buried in the capsule wall and thus unable to provide the required ‘gate’ (Fig. 5b). However, use of a maleic anhydride acid linker greatly improved the microstructure, with the microspheres penetrating but sitting mostly on the outside of the capsule wall (Fig. 5c). In order to optimize this system, it was important to determine the distribution of the acid linker. For optimum effectiveness, it should sit only at the outer surface of the microspheres to assist in forming the interface to the capsule wall. Analysis of a C1s STXM image sequence recorded from a thin section

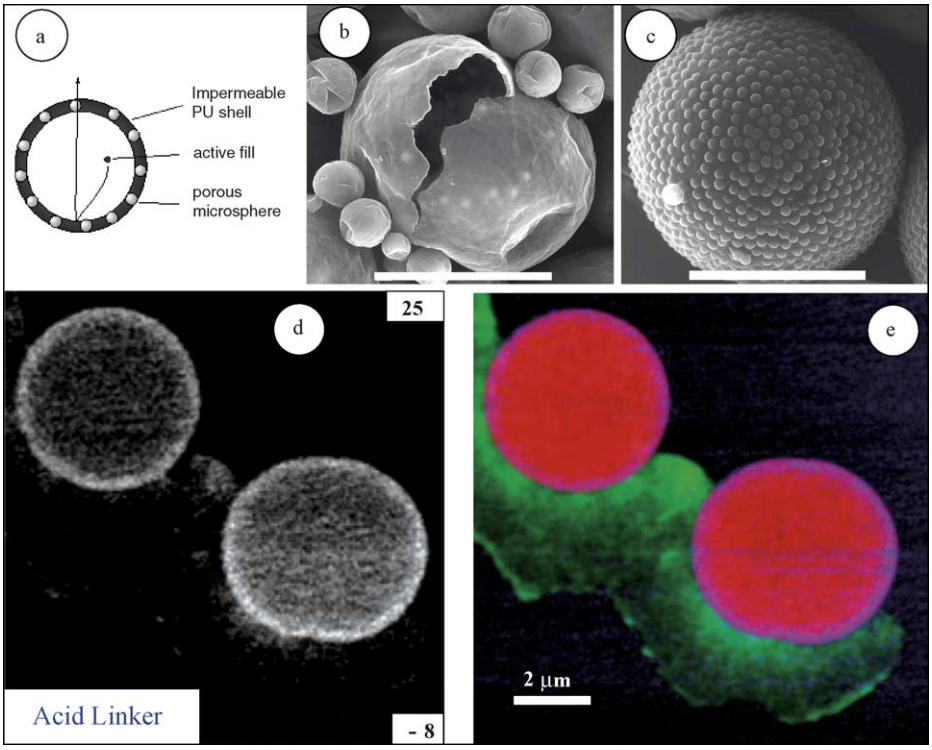


Fig. 5. (a) Sketch of the 'tectocapsule' concept. The capsule wall should be impermeable while partial permeability of the embedded microcapsules allows slow release. (b) Simple combination results in microspheres without external contact (SEM image). (c) Addition of maleic anhydride, a covalently linked compatibilizer, to the DVB-55 microspheres produces tectocapsules with the desired exterior contact (SEM, scale bar = 100 μm). (d) Component map of the acid linker derived from fits using an internal model taken from the edge of the microspheres. (d) Color composite indicating location of compatibilizer relative to the polyurea capsule (green) and DVB-55 microsphere (red) (recorded with STXM5.3.2).

of an epoxy-embedded capsule provided a map of the acid linker (Fig. 5d and e) which was found to be well localized, as required [36]. The compatibilizer has a local concentration in the outer 100–200 nm of the microsphere of 5–10% but overall it is much less than 0.1% of the sample. A large number of other synthetic polymer microstructure systems have been examined by STXM, many of them with direct industrial relevance. The unique analytical power and added value of STXM for feedback in optimization of synthetic polymer systems is very clear.

## 6. Surface analysis by soft X-ray spectromicroscopy

Biomaterials used for medical applications are often polymers, either in the bulk, to form structures with desired mechanical properties (e.g. flexible dialysis tubes), or as coatings, to provide required chemical and biochemical properties (protein repellency, hydrophilicity, etc.). Control of the location and type of proteins adsorbed on first contact of a biomaterial with bodily fluids is a goal of much biomaterials development. Optimization of polymer systems to achieve biocompatibility while providing necessary structural support and flexibility is a very active area of research and new techniques, which can offer improved sensitivity are always of interest. We are developing both STXM and PEEM for applications in biomaterials optimization. Ideally, one wants to quantitatively map proteins, cells or other biological substances adsorbed on the surface of laterally heterogeneous substrates, under a layer of the bodily fluid of interest (blood plasma, intercellular fluid, tears, etc.). For this the ability of STXM to examine samples through an aqueous overlayer is particularly attractive. Although STXM sums the signal through the whole column examined and thus has no intrinsic surface sensitivity, with sufficient NEXAFS chemical contrast minority components, such as surface adsorbates can be mapped. Typically, if the surface signal is of the order of 1% of the total signal, it is feasible to use STXM for surface studies. Recently, we have used STXM to show that fibrinogen (Fg) is preferentially adsorbed at the interface of styrene–acrylonitrile filler particles and a polyether matrix when a filler-particle polyurethane sample is exposed to a dilute buffered solution of fibrinogen, and then imaged in three different forms: dry, with an overlayer of distilled water, and with a thin overlayer of dilute protein buffer solution (at 0.01 mg/ml) [38].

In the X-PEEM instrument at ALS beamline 7.3.1 [6], a 30 μm diameter X-ray beam strikes the surface at 15° incidence. Primary and secondary photo-ejected electrons, extracted into an electrostatic imaging system by a strong elec-

tric field (∼10 kV/mm) at the sample, are used to form a magnified image at a phosphor screen, which is then recorded with a CCD camera. The spatial resolution can be as good as 50 nm, although it is more typically 100 nm for studies of polymer thin films due to the need to reduce flux to minimize radiation damage. Samples for X-PEEM must be conducting, very flat (<1 μm roughness, without sharp discontinuities that can cause field emission) and UHV-compatible (no outgassing). Images are recorded at one or more photon energies, and image sequences are used for spectral acquisition. The X-PEEM sampling depth, ∼5 nm for C 1s studies of soft matter (this value depends on the material and photon energy), is very similar to the size of the large protein or polysaccharide macromolecules that are involved in cell attachment, foreign body recognition etc. Thus, X-PEEM is well suited to biomaterials studies. It has several major drawbacks, such as requirement of vacuum compatibility, and adequate conductivity of the sample to avoid charging. However, many other vacuum techniques are routinely used for biomaterials studies – X-ray photoelectron spectroscopy, secondary ion mass spectrometry, electron microscopy etc. – and thus, with appropriate precautions, it is reasonable to expect X-PEEM can provide relevant information about protein biomaterial surface interactions.

Blends of polystyrene (PS) and polymethylmethacrylate (PMMA) are being used as model substrates for investigating preferential protein attachment. We have used atomic force microscopy (AFM), STXM and X-PEEM to investigate phase segregation in spun cast thin films of PS/PMMA blends [39], and the interaction of fibrinogen with the laterally differentiated PS/PMMA surfaces [40]. Fig. 6 presents OD images of a ∼40 nm PS/PMMA thin film recorded with STXM5.3.2. The film was initially spun cast from a 1% toluene solution onto freshly cleaved mica, transferred to the surface of ultra-pure water then to a silicon nitride window, and vacuum annealed at 160 °C for 8 h. The high degree of phase segregation into PS and PMMA domains is obvious from images at the two high contrast energies (Fig. 6a and b). At all other energies, there is little or no contrast. Analysis of the C 1s spectra of the PMMA domains (Fig. 6d) show them to be quite pure, with less than 3% of the signal arising from PS. The small PS signal arises from very small micro-domains of pure PS trapped in the PMMA macro-domains. Fig. 6c shows an expanded image, which shows a PMMA micro-domain in PS and (lower

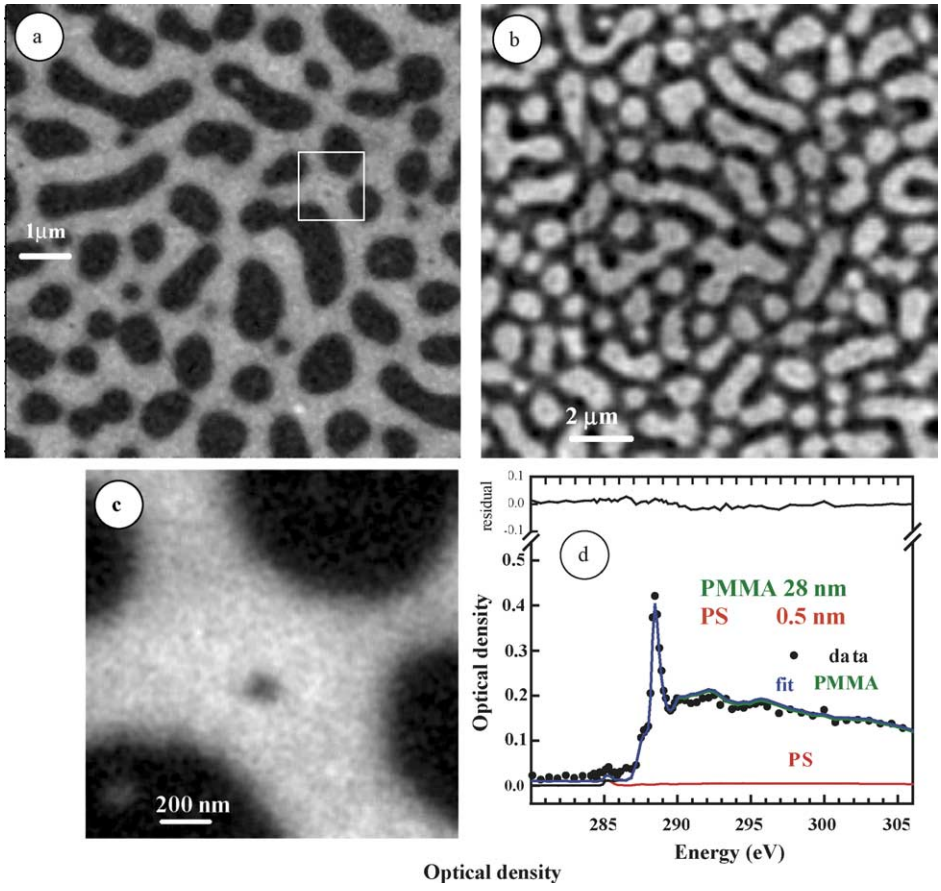


Fig. 6. (a) OD image (285.1 eV) of a ∼40 nm PS/PMMA thin film spun cast on a Si wafer recorded with STXM5.3.2. (b) OD image (288.4 eV) recorded after a 67 energy image sequence (for a total of ∼70 ms at each pixel, ∼10 MGy dose). The radiation damage from the image sequence is very small and only visible at this energy. (c) Expansion of Fig. (6a) measurement showing a ∼100 nm PMMA micro-domain trapped in a PS macro-domain. (d) Fit to the spectrum of the PMMA domain. The 2% PS component arises from PS micro-domains (recorded with STXM5.3.2).

left) a PS micro-domain in PMMA. One issue of continual concern in soft X-ray microscopy is radiation damage. The 288.4 eV image (Fig. 6b), recorded after a 67 energy image sequence (~70 ms exposure at each pixel, ~10 MGy dose), shows that the analytical measurement does cause detectible damage, but this is very small. Analysis of the image contrast indicates the damage reduces the C 1s → $\pi^*$ C=O transition intensity by only 5% of the spectral change at saturation damage [41]. The beam damage was only visible at this particular photon energy, indicating negligible mass loss has occurred. In general, it is important to characterize dose–damage relationships [41] and to use the minimum practical measurement doses. Typically, we try to keep the exposure to less than 20% of the half-time for the fastest damage process, although longer exposures are sometimes needed to obtain adequate statistics, and can be justified in that, although the most sensitive component may be modified in the measurement, the additional signal allows more confident mapping of another component which damages at a slower rate. This is the situation for the acquisition strategy used for X-PEEM detection of fibrinogen adsorbed on PS/PMMA [40].

PS/PMMA thin film blends on Si or $Si_3N_4$, have been used as a substrate for systematic studies of the adsorption of fibrinogen. While PS and PMMA have similar hydrophobicity, the polarizablity and hydrogen bonding capability differs so it is reasonable to expect some difference in the affinity of a protein for these two species. Indeed, adsorption isotherms measured on pure PS and PMMA with $^{125}I$ radioactive labeling [40] show that fibrinogen has a higher affinity for PS. The question that X-ray microscopy can address is whether the adsorption is dictated by thermodynamics or by kinetics, since a different site might be kinetically favored. When adsorption is carried out from dilute phosphate buffered solutions X-PEEM shows that fibrinogen prefers to adsorb on the PS domain, as predicted from the radio-labeling studies [40]. However, when the adsorption is performed from a non-buffered aqueous solution, the fibrinogen shows a clear preference for adsorption at the interface of the PS and PMMA domains. Fig. 7 shows C 1s and N 1s X-PEEM results for adsorption of fibrinogen from deionized water at two different concentrations. Fig. 7a is the color composite derived from a C 1s image sequence for adsorption from a 0.05 mg/ml Fg solution. It suggests that Fg prefers to adsorb at the interface of the PS and PMMA domains, rather than preferring either domain alone. The spectra of high-PS, high-PMMA and high-Fg regions extracted from regions defined by threshold masking the individual component maps are shown in Fig. 7b. These spectra show that the signal from the interface (blue) is a composite of PS, Fg and PMMA, while the spectra of the PS (red) and PMMA (green) domains are relatively pure signatures of the dominant species. Fig. 7c and d are results from analysis of a N 1s image sequence recorded for adsorption from a 0.1 mg/ml Fg unbuffered aqueous solution. As with the C 1s measurement, the N 1s signal of fibrinogen is found

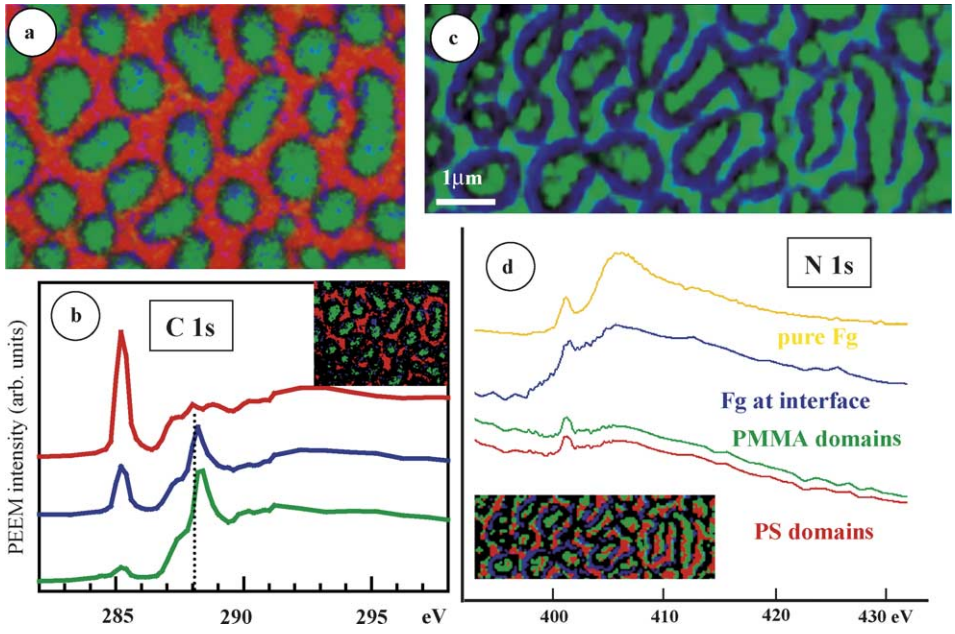


Fig. 7. (a) Color coded composite map (PS: red, PMMA: green, Fg: blue) of a PS/PMMA thin film (40 nm thick on a Si wafer), exposed for 10 min to a 0.05 mg/ml aqueous solution of Fg, derived from a C 1s X-PEEM image sequence. (b) C 1s spectra extracted from the image sequence by regions defined as PS-rich (red), PMMA-rich (green) and Fg-rich (blue) from a threshold masking (~top 20% of signal) of the component maps. (c) Color coded composite map (PS: red, PMMA: green, Fg: blue) of a PS/PMMA thin film (40 nm thick on a Si wafer), exposed for 10 min to a 0.1 mg/ml aqueous solution of Fg, derived from a N 1s PEEM image sequence. (d) N 1s spectra of regions defined as Fg-rich (blue), PS-rich (red), PMMA-rich (green) identified by threshold masking (~top 20% of signal) of the Fg component map, the non-Fg component map and the inverse of the non-Fg map (the non-Fg map shows the PS and PMMA domains, probably by topographic contrast). The insets in (b) and (d) indicate the regions from which the spectra were obtained (recorded with ALS PEEM-2).

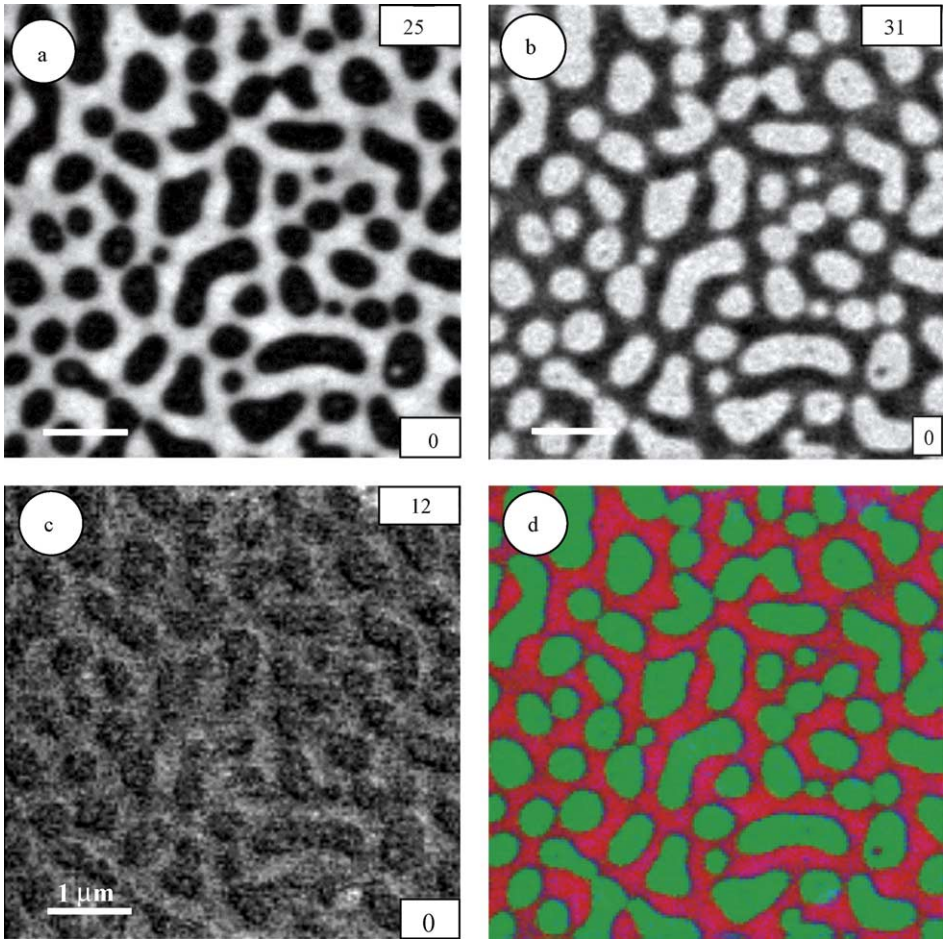


Fig. 8. (a) PS, (b) PMMA, and (c) albumin component maps and (d) color composite derived from a C 1s image sequence from a 40 nm PS–PMMA thin film on a $Si_3N_4$ window exposed to a 0.02 mg/ml aqueous solution of human serum albumin. Excess protein solution was washed off prior to drying and measuring the sample. The numbers on the right hand side indicate grayscale thickness limits in nanometer (recorded with STXM5.3.2).

at the interface of the PS and PMMA domains. Although a small protein-like N 1s signal is found in spectra extracted from the PS and PMMA domains, this is only about 10% of the signal found at the interface. When the spectrum of the interface is compared to the N 1s spectrum of pure Fg (Fig. 7d), there is additional intensity around 399–400 eV. These differences most likely indicate radiation damage, which is known to reduce the intensity of the 401.2 eV transition and form a damage product with signal below 400 eV [41].

Fig. 8 shows results from analysis of a C 1s image sequence recorded using STXM for a sample consisting of a PS/PMMA thin film blend (on $Si_3N_4$) exposed for 10 min to a 0.02 mg/ml solution of albumin in deionized water, then rinsed to remove non-adsorbed protein. Again, it is clear that the protein preferentially adsorbs at the interface. This is perhaps not surprising as proteins have multiple sites for attachment, and the PS/PMMA interface may offer more favorable sites than just pure PS or pure PMMA. What is significant about this example is that protein can be detected and mapped with the 'bulk-sensitive' STXM technique at monolayer levels similar to those detected in PEEM.

## 7. Summary

The field of soft X-ray spectromicroscopy is very young and there are countless opportunities for further improvements in instrumentation, data analysis, and novel applications. Although access is still somewhat limited, as more third generation synchrotron facilities come on line additional microscopes will be built and there will be more opportunities for new users to join this field. Trends in recent and future developments include: in situ sample modifications such as gas–surface reactions, thermal processing, strain, electrochemistry, etc.; three dimensional chemical mapping [42]; further improvements in spatial resolution through better zone plates [43], and use of scanning probe tips as localized detectors of photo-ejected electrons [44].

## Acknowledgements

Measurements performed at beamlines 5.3.2, 11.0.2 and 7.3.1 at the Advanced Light Source, funded by DoE un-

der contract DE-AC03-76SF00098. Research supported by NSERC (Canada), AFMnet (Advanced Food and Biomaterials Network), the Canada Research Chair program (Hitchcock), and 3M Canada, through the 3M Industrial chair (Stöver). Zone plates at ALS were provided by CXRO, LBNL. We thank Tolek Tyliszczak and David Kilcoyne for their excellent work in developing and maintaining STXM5.3.2, Andreas Scholl and Andrew Doran for help with operating PEEM2 at the ALS, Marcia West for excellent microtomy, and George Swerhone for preparing the biofilm wet cell samples.

## References

[1] J. Stöhr, NEXAFS Spectroscopy, Springer-Verlag, Berlin, 1992.
[2] J. Kirz, C. Jacobsen, M.Q. Howells, Q. Rev. Biophys. 28 (1995) 33.
[3] G. Schneider, Ultramicroscopy 75 (1998) 85.
[4] E. Bauer, J. Electron Spectrosc. Relat. Phenom. 114–116 (2001) 976.
[5] E. Bauer, J Phys.: Condens. Matter 13 (2001) 11391.
[6] S. Anders, H.A. Padmore, R.M. Duarte, T. Renner, T. Stammler, A. Scholl, M.R. Scheinfein, J. Stöhr, L. Séve, B. Sinkovic, Rev. Sci. Instrum. 70 (1999) 3973.
[7] H. Ade, in: J.A.R. Samson, D.L. Ederer (Eds.), Experimental Methods in the Physical Sciences, vol. 32, Academic Press, 1998, p. 225.
[8] S.G. Urquhart, H. Ade, Chemical Applications of Synchrotron Radaition, vol. 285, 2002, p. 285.
[9] J. Susini, D. Joyeux, F. Polack (Eds.), Proceedings of the Seventh International Conference X-ray Microscopy, J. de Physique 104 (2003).
[10] C. Jacobsen, S. Wirick, G. Flynn, C. Zimba, J. Microsc. 197 (2000) 173.
[11] A.L.D. Kilcoyne, T. Tyliszczak, W.F. Steele, S. Fakra, P. Hitchcock, K. Franck, E. Anderson, B. Harteneck, E.G. Rightor, G.E. Mitchell, A.P. Hitchcock, L. Yang, T. Warwick, H. Ade, J. Synchrotron Radiat. 10 (2003) 125.
[12] T. Warwick, H. Ade, A.L.D. Kilcoyne, M. Kritscher, T. Tylisczcak, S. Fakra, A.P. Hitchcock, P. Hitchcock, H.A. Padmore, J. Synchrotron Radiat. 9 (2002) 254.
[13] T. Tyliszczak, H.A. De, S. Fakra, B. Harteneck, A.P. Hitchcock, J. Dynes, J.R. Lawrence, T. Araki, A. Nilsson, S. Miyeni, A.L.D. Kilcoyne, J.A. Liddle, D.K. Shuh, T. Warwick, J. Electron Spectrosc. Relat. Phenom., in preparation.
[14] B.L. Henke, E.M. Gullikson, J.C. Davis, At. Data Nucl. Data Tables 54 (1993) 181.
[15] aXis2000 written in interactive data language (see www.rsinc.com), is available at http://unicorn.mcmaster.ca/aXis2000.html.
[16] H. Ade, X. Zhang, S. Cameron, C. Costello, J. Kirz, S. Williams, Science 258 (1992) 972.
[17] X. Zhang, R. Balhorn, J. Mazrimas, J. Kirz, J. Struct. Biol. 116 (1996) 355.
[18] I.N. Koprinarov, A.P. Hitchcock, C. McCrory, R.F. Childs, J. Phys. Chem. B 106 (2002) 5358.
[19] W.-H. Li, H.D.H. Stöver, J. Polym. Sci., Polym. Chem. 37 (1999) 2295.
[20] I.N. Koprinarov, A.P. Hitchcock, W.H. Li, Y.M. Heng, H.D.H. Stöver, Macromolecules 34 (2001) 4424.
[21] G. Zheng, L.M. Croll, A.P. Hitchcock, H.D.H. Stöver, in preparation.
[22] N. Bonnet, J. Microsc. 190 (1998) 2.
[23] A. Osanna, C. Jacobsen, AIP Conf. Proc. 507 (2000) 350.
[24] M. Lerotic, C. Jacobsen, T. Schäfer, S. Vogt, Ultramicroscopy 100 (2004) 35.;
M. Lerotic et al., J. Electron Spectrosc. Relat. Phenom., these proceedings.
[25] T.R. Neu, G.D.W. Swerhone, J.R. Lawrence, Microbiology 147 (2001) 299.
[26] J.R. Lawrence, D.R. Korber, G.M. Wolfaardt, D.E. Caldwell, T.R. Neu, Analytical imaging and microscopy techniques, in: C.J. Hurst, R.L. Crawford, G.R. Knudsen, M. McInerney, L.D. Stetzenbach (Eds.), Manual of Environmental Microbiology, second ed., American Society for Microbiology Press, Washington, DC, 2002, pp. 39–61.
[27] J.R. Lawrence, G.D.W. Swerhone, G.G. Leppard, T. Araki, X. Zhang, M.M. West, A.P. Hitchcock, Appl. Environ. Microbiol. 69 (2003) 5543.
[28] J. Rothe, E.M. Kneedler, K.H. Pecher, B.P. Tonner, K.H. Nealson, T. Grundl, W. Meyer-Ilse, T. Warwick, J. Synchrotron Radiat. 6 (1999) 359.
[29] K.H. Pecher, D.M. McCubbery, E.M. Kneedler, J. Rothe, J.R. Bargar, G. Meigs, L. Cox, K.H. Nealson, B.P. Tonner, Geochim. Cosmochim. Acta 67 (2003) 1089.
[30] E.S. Gilbert, A. Khlebnikov, W. Meyer-Ilse, J.D. Keasling, Water Sci. Technol. 39 (1999) 269.
[31] C.S. Chan, G. De Stasio, S.A. Welch, M. Girasole, B.H. Frazer, M.V. Nesterova, S. Fakra, J.F. Banfeld, Science 303 (2004) 1656.
[32] R. Arshady (Ed.), Microspheres, Microcapsules, Liposomes: vol 1. Preparation and Applications, Citrus Books, London, 1999.
[33] T. Araki, A.P. Hitchcock, F. Shen, P. Chang, M. Wang, R.F. Childs, J. Biomater. Polym. Ed., 2005, in press.
[34] M. Okubo, J. Izumi, R. Takekoh, Colloid Polym. Sci. 27 (1999) 875.
[35] R. Takekoh, M. Okubo, T. Araki, H.D.H. Stöver, A.P. Hitchcock, Macromolecules 38 (2005) 542.
[36] L.M. Croll, H.D.H. Stöver, A.P. Hitchcock, Macromolecules, in press.
[37] L.M. Croll, H.D.H. Stöver, Langmuir 19 (2003) 5918.
[38] A.P. Hitchcock, C. Morin, Y.M. Heng, R.M. Cornelius, J.L. Brash, J. Biomater. Sci. Polym. Ed. 13 (2002) 919.
[39] C. Morin, H. Ikeura-Sekiguchi, T. Tyliszczak, R. Cornelius, J.L. Brash, A.P. Hitchcock, A. Scholl, F. Nolting, G. Appel, A.D. Winesett, K. Kaznacheyev, H. Ade, J. Electron Spectrosc. 121 (2001) 203.
[40] C. Morin, A.P. Hitchcock, R.M. Cornelius, J.L. Brash, A. Scholl, A. Doran, J. Electron Spectrosc. 137–140 (2004) 785.
[41] C. Morin, L. Li, A.P. Hitchcock, A. Doran, A. Scholl, J. Electron Spectrosc., in preparation.
[42] A.P. Hitchcock, T. Araki, H. Ikeura-Sekiguchi, N. Iwata, K. Tani, J. Phys. IV 104 (2003) 509 (France).
[43] T. Warwick, H. Ade, S. Fakra, M. Gilles, A.P. Hitchcock, A.L.D. Kilcoyne, D. Shuh, T. Tylisczcak, Synchrotron Radiat. News 16 (2003) 53.
[44] T. Matsushima, T. Okuda, T. Eguchi, M. Ono, A. Harasawa, T. Wakita, A. Kataoka, M. Hamada, A.I. Kamoshida, Y. Hasegawa, T. Kinoshita, Rev. Sci. Inst. 75 (2004) 2149.